RICE UNIVERSITY

Studies of the $5s^2\ {}^1S_0$ - $5s5p\ {}^3P_1$ Transition in Atomic Strontium

by

Yenny Natali Martinez

A Thesis Submitted
in Partial Fulfillment of the
Requirements for the Degree

Master of Science

Approved, Thesis Committee:

Thomas C. Killian, Chairman
Assistant Professor of Physics and
Astronomy

Randall G. Hulet
Fayez Sarofim Professor of Physics and
Astronomy

James P. Hannon
Professor of Physics and Astronomy

Houston, Texas

April, 2008

ABSTRACT

Studies of the $5s^2\ {}^1S_0$ - 5s5p ${}^3P_1$ Transition in Atomic Strontium

by

Yenny Natali Martinez

This research utilizes the Electron Shelving (ES) technique to obtain a lifetime measurement of the ${}^3P_1$ energy state of strontium. The $5s^2 {}^1S_0 \rightarrow 5p\ {}^3P_1$ intercombination transition is important because of its promising usefulness in optical frequency standards and high resolution spectroscopy. Unfortunately, the transition lacks a high photon scattering rate to produce a significant signal for optical studies and therefore it is advantageous to monitor the vastly stronger ${}^1S_0 \rightarrow {}^1P_1$ transition. This lifetime measurement yielded a value of $\tau = 23 \pm 3\ \mu$s (systematic uncertainty), which is longer than other current experimental values established in literature. Additional lineshape studies with a dependence on magnetic fields, gravitational acceleration, and laser power were performed and are discussed briefly. These lineshape studies allow an upper linewidth limit to be placed on the pumping laser causing this transition, making these secondary studies a useful method to characterize the laser.

Acknowledgments

How grateful I am to be able to thank those who have helped me complete this work – unfortunately, I won't be able to name everyone.

Dr. Killian, I still can't call you Tom. No one has had a better advisor than I have. I am deeply indebted to you for your knowledge, patience, drive which have guided me up to this point in my graduate career. I want to thank Dr. Randy Hulet and Dr. James Hannon for your meticulous reading of my thesis drafts. And I am ironically grateful for your elevated requirements for me to earn this degree. Thank you very much for taking the time that you did to help me write a complete thesis. And I can't forget Dr. Han Pu. I could not have prepared for my defense without you. I am so grateful for your humble wisdom and patience with me as I tried to understand the topics in AMO physics. These are not the only professors that have impacted my professional studies. I could never name all of the mentors I have had and am grateful for throughout my university years.

I want to thank my laboratory partners for becoming my family. Clayton, for treating me like a sister; Sarah for sharing many emotional and sacred feelings with me; Sampad for being so calm and making me feel calm; Priya for being so free and exuberant; Pascal for his sardonic wit; and Aaron for being so confident and hardworking. I don't mean any of these things the wrong way – if you know me I

hope you know this.

Y hoy quiero agradecerles a las personas más íntimas de mi vida. A nadie en este mundo le puedo agradecer más que a mi madre. Mamá, usted ha sacrificado todo en su vida por mí y por mis hermanos y nunca terminaré de agradecerle. Padre mío, a usted le debo mis ancias de aprender. ¿Cómo sabría yo de niña que lo poco que estoy logrando hoy es fruto de su esfuerzo por enseñarme a trabajar y a aprender? Lo único que puedo y quiero hacer es honrarles con mi vida. Y mis queridos hermanos—tres hombres excelentes. Me siento inmensamente feliz por el progreso de los tres. Gracias, hermanos mios, por ser celosos conmigo y por quererme.

Quiero agradecerle a Lourdes por ser mi mano derecha. A todas mis queridas amigas, amigos y segundos padres que tengo en mi vida. Y a mi Padre, porque nadie sabrá cuanto me costo esto mejor que Él.

Contents

Abstract ii

Acknowledgments iii

List of Figures vii

1 Introduction 1

1.1 The $^1S_0 \rightarrow {}^3P_1$ Transition 2

1.2 Dipole-Allowed Versus Intercombination Transitions 4

1.3 Importance of This Atomic Transition 5

1.4 Summary of Chapters 8

2 Atomic Structure Calculations 9

3 Electron Shelving technique 12

3.1 Naive Experimental Setup 12

3.2 Idea of the Electron Shelving Technique 13

3.3 Absorption Method 15

3.4 Background of the ES Technique 18

4 Lifetime Measurements 20

4.1 Experimental Procedure 20

4.2 Determining the Resonance Frequency 25

5 Discussion and Conclusion **27**

5.1 Optical Depth Considerations 28

5.2 Laser Drift Considerations 31

5.3 Other Observations 33

5.4 Discussion of Measurement 35

5.5 Comparison with Literature 36

A Lineshape Studies of the $^1S_0 \rightarrow {}^3P_1$ Transition **41**

A.1 Magnetic Field Effect 42

A.2 Time-of-flight Effect 42

A.3 Power Effect 44

References **46**

List of Figures

1.1 Energy level diagram of strontium 3

3.1 Schematic of 689 nm fluorescence experiment 13

3.2 A three-level Sr atom to describe the ES technique 13

3.3 A sample absorption image 16

3.4 Comparison of the number of atoms obtained through two methods of data analysis 18

4.1 Experimental setup for lifetime measurements 21

4.2 Experimental timing sequence for lifetime measurements 22

4.3 Sample lifetime data and fit 24

4.4 Spectrum curve for determining the resonance frequency 25

5.1 Compilation of lifetime values for all experimental days 27

5.2 Lifetime values with image beam detuning indicated 29

5.3 Number of atoms versus peak OD with image beam detuning indicated 30

5.4 Lifetime values versus peak OD with image beam detuning indicated 30

5.5 Plot of lifetime curve with time elapsed between data points distinguished 32

A.1 Effect of external magnetic field on the linewidth of the $^1S_0 \rightarrow {}^3P_1$ transition 43

A.2 Effect of time-of-flight variation on the linewidth of the $^1S_0 \rightarrow {}^3P_1$ transition 44

A.3 Laser power effect on the linewidth of $^1S_0 \rightarrow {}^3P_1$ transition 45

Chapter 1
Introduction

This thesis presents a lifetime measurement of the $^3P_1$ state in atomic strontium, during which the difficulty of measuring the very weak $^1S_0 \rightarrow {}^3P_1$ intercombination line signal is overcome by monitoring the stronger $^1S_0 \rightarrow {}^1P_1$ transition. The experimental technique used to detect the dynamics of the system is called electron-shelving [1, 2].

Alkali-metal atoms were the first to be used for laser cooling and trapping experiments. Two major reasons account for this choice of atoms: most alkalis have a high vapor pressure at modest temperatures (on the order of 100 degrees Celsius), and their strong cycling transition is in the visible or near IR range of radiation, making lasers and imaging systems readily available [3]. However, cooling and trapping of alkaline-earth and ytterbium (Yb) atoms was soon possible as well. These atoms are intriguing because of their often simpler atomic level structure, potential use in optical frequency standards, and demand for more complete atomic structure calculations.

Strontium (Sr), an alkaline-earth atom, is rigorously studied experimentally and theoretically for these reasons. The first experimental laser cooling of Sr was performed by Kurosu and Shimizu in 1990 [4]. Since then, Sr has been the topic of

narrow-line cooling [5], optical frequency standards [6], and cold collision studies [7, 8]. For all of these applications and more, fundamental characteristics of Sr need to be determined through experiment and theory. One of the most valuable quantities that can be measured for an atom are the lifetimes of its energy levels because, for example, it is a direct measure of the reduced matrix element between atomic states.

Previous lifetime measurements of strontium's $^3P_1$ state have been obtained through various experimental methods including the hook method [9] and atomic beam techniques [10]. More current experimental values were obtained by time-resolved fluorescence detection after laser excitation (for example, see Drozdowski et al. [11]). The most current theoretical values were computed by Porsev et al. [12, 13], Savukov and Johnson [14], and Santra et al. [15], to name a few.

The rest of Chapter 1 gives an overview of the $^1S_0 \rightarrow {}^3P_1$ transition, why it is different from normal broadband transitions, and its importance.

1.1 The $^1S_0 \rightarrow {}^3P_1$ Transition

One of the strongest reasons strontium has attracted interest is because of its $^1S_0 \rightarrow {}^3P_1$ transition. Alkaline-earth metal atoms have isotopes that possess no nuclear spin ($I = 0$) and therefore, no hyperfine structure. Because of the two valence electrons, energy levels can form singlet ($S = 0$) or triplet ($S = 1$) states, depending on the coupling of the electron spins. As described in Section 1.2, these level manifolds mix and produce transitions known as "intercombination" transitions.

Such transitions are characterized by narrow linewidths and rather long lifetimes. For Sr, one of these transitions occurs at a vacuum wavelength of 689.45 nm, and the $^3P_1$ state has a lifetime of about 21 μs. The corresponding linewidth is $\gamma/2\pi = 7.6$ kHz. The energy level diagram showing relevant levels is displayed in Figure 1.1. In this figure, other states that are optically coupled to the $^3P_1$ state are also shown.

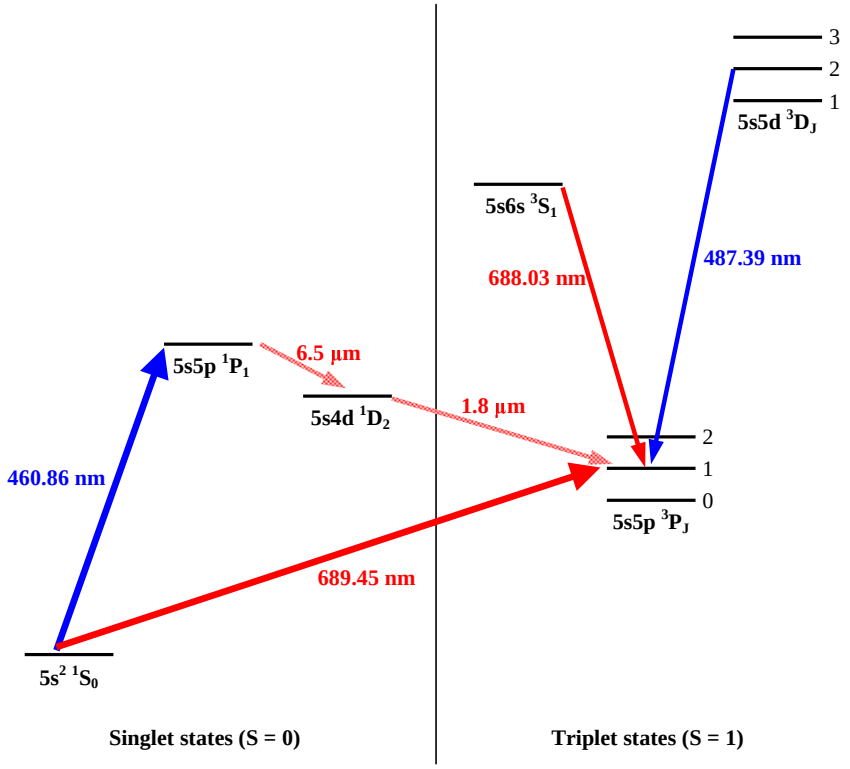

Figure 1.1 A simplified energy level diagram for ^{88}Sr, showing relevant transitions and their vacuum wavelengths. The states are separated into singlet and triplet states. The total angular momentum J of the state is specified to the right of the state for the triplet groups. The 461 nm and 689 nm (intercombination line) transitions are used for laser cooling for the work of this thesis. Adapted from [16, 17].

1.2 Dipole-Allowed Versus Intercombination Transitions

Most atomic transitions are electric dipole allowed (E1) transitions which obey the $\Delta S = 0$ dipole selection rule. These transitions are characterized by linewidths on the order of tens of MHz and lifetimes in the nanosecond range. However, as the atomic mass increases, there is a LS-coupling breakdown, and spin-orbit and other relativistic effects induce mixing of states with the same total angular momentum J and different spin S [18]. In the case of Sr, the small amount of $S = 0$ $^1P_1$ state mixed into the $^3P_1$ state allows the $\Delta S = 1$ transition to support dipole transitions. This condition, in which a spin-forbidden transition can support E1 transitions, brings about interesting differences between intercombination and dipole allowed transitions. The singlet and triplet labels used for different energy levels are only approximate, but they will be used by convention.

A very important difference to note between dipole allowed and intercombination transitions is their rate of photon scattering in a laser field. The rate of spontaneous emission R, which is analogous to photon scattering, is given by [3]

$$R = \frac{\frac{I}{I_s}\frac{\gamma}{2}}{1 + \frac{I}{I_s} + (\frac{2\Delta}{\gamma})^2} \tag{1.1}$$

where γ is the natural linewidth of the energy state, I is the intensity of the laser incident on the atoms, $I_s = 2\pi^2 c\hbar\gamma/3\lambda^3$ is the saturation intensity, and Δ is the laser detuning from the transition frequency. The maximum rate of scatter is $\gamma/2$, so one can see that the intercombination line scatters less efficiently than the dipole

transition. This maximum rate translates to 10^3 photons per atom per second while, for E1 transitions, the rate is on the order of 10^8. Therefore, fluorescence signals are much stronger for broad transitions.

Another distinction between these two types of transitions is the laser-cooling temperature limit. For atoms such as the bosonic isotope of Sr with nondegenerate ground states, laser cooling is well described by Doppler cooling [3], and the temperature limit is $\mathrm{T}_D = \frac{h\gamma}{2k_B}$. The broad transitions, with energy widths of the excited state around 30 MHz, correspond to a temperature on the order of 1 mK. On the other hand, the intercombination line has a theoretical Doppler temperature of $\mathrm{T}_D = 180$ nK.

At the ultracold temperatures of intercombination line cooling, the temperature is actually limited by the photon recoil. Conventionally $\mathrm{T}_r \equiv \frac{2E_r}{k_B}$, where $\mathrm{E}_r = \frac{\hbar^2 k^2}{2m}$, and the lowest limit attainable for Doppler cooling with $h\gamma \ll E_r$ is $\mathrm{T}_r/2$ [19, 20]. The narrow $^1S_0 \rightarrow {}^3P_1$ transition has a recoil temperature of $\mathrm{T}_r = 460$ nK. This is the major distinction in the temperature limits between dipole allowed and intercombination transitions: the temperature limit for narrow lines becomes the half the recoil limit, while the opposite is true for broad transitions.

1.3 Importance of This Atomic Transition

The $^1S_0 \rightarrow {}^3P_1$ transition has attracted much attention from other experimental and theoretical groups because of its laser cooling and trapping properties. Narrow

line cooling on this transition was first performed by Katori et al. in 1999 [5]. Using this line, they achieved the lowest Sr MOT temperature of 400 nK with a density of over 10^{12} cm^{-3}. Since then, other groups [5, 21, 22] have achieved MOTs using this transition, including the Killian lab in 2004 [8].

Alkaline-earth atoms and Yb are interesting for many reasons, one of which is for optical frequency standards. Research using calcium shows that its $^1S_0 \rightarrow {}^3P_1$ transition can be used for an optical atomic clock [23–25]. ^{87}Sr has a $^1S_0 \rightarrow {}^3P_0$ transition with a natural linewidth of 1 mHz that has been explored as a potential "optical lattice clock" [26]. The ^{88}Sr $^1S_0 \rightarrow {}^3P_1$ transition was recently investigated in a perturbation-free regime [27] and may offer an improvement over the cesium atomic clock, the current frequency standard [28].

Because of its narrow frequency requirements, using the $^1S_0 \rightarrow {}^3P_1$ transition requires better laser technology than that necessary for broad transitions. Particularly for the Killian laboratory, in which the 689 nm pumping laser used to excite atoms to the $^3P_1$ state was hand built, laser cooling results are dictated by the laser's performance. This atomic transition can help as a tool for the characterization of the pumping laser, as the experiments described in Appendix A show.

The main use of this transition in the Killian group is for narrow linewidth laser cooling. Transferring the 461 nm MOT atoms to a second-stage MOT made up of 689 nm beams gives colder atoms than in the 461 nm MOT alone. Temperatures as

low as 2 μK have been observed after this two-stage cooling. From this colder, denser MOT, photoassociative spectroscopy (PAS) experiments resulted [8]. The atoms' low temperatures provide the largest signal possible because there is no significant Doppler broadening and because collisions caused by the 461 nm PAS laser are s-wave collisions. Through the PAS experiments, important parameters necessary to allow other experiments have been determined (such as the scattering length of both ^{88}Sr and ^{86}Sr [29]). PAS and other cold collision studies rest upon the initial conditions provided by narrow linewidth laser cooling.

Quantum degeneracy studies have been theorized to be possible by beginning with the cold, dense MOT available through this transition. Transferring 689 nm MOT atoms into a dipole trap is hypothesized to cause the atoms to reach phase-space densities necessary for Bose-Einstein condensation (BEC) of bosonic Sr atoms [5, 30]. BEC was recently realized in Yb by a very similar setup, in which two-stage cooled atoms were transferred into an optical dipole trap and evaporatively cooled [31].

The complexity of the atomic structure of alkaline-earth metal atoms, due to its two valence electrons, requires better atomic models and calculations than those currently available. This topic will be discussed in greater depth in Chapter 2.

The study of this transition is motivated by the reasons described above. An important step to take in the study of this transition is to obtain an accurate and precise measurement of the $^3P_1$ state lifetime. The work presented in this thesis

describes this lifetime measurement.

1.4 Summary of Chapters

The remainder of this thesis is organized as follows: The motivation for better atomic structure calculations is discussed in Chapter 2. This will be followed in Chapter 3 by a description of the electron shelving method, an established technique used to monitor the weak intercombination transition through the $^1S_0 \rightarrow {}^1P_1$ signal. This chapter also includes a description of the image analysis performed for the lifetime measurement. Chapter 4 presents the lifetime measurement experiment. A discussion of the measured value, the possible systematic problems encountered in the lifetime experiment, a comparison of our value to current experimental and theoretical values, and a note on future work is contained in Chapter 5. Finally, additional lineshape studies performed during data taking are presented in Appendix A.

Chapter 2
Atomic Structure Calculations

The lifetime of an atomic state can be calculated from first principles. A Hamiltonian is constructed that describes the atomic system. Then, the eigenstates and eigenvectors of this system are found for this Hamiltonian. The lifetime is then related to the dipole matrix elements between the atomic state and lower-lying states. One can compare this theoretical value to measurements acquired through experiments, such as the lifetime measurement presented in this thesis, to refine theory. Conversely, theory can calculate parameters, such as molecular potential parameters and hyperfine shifts, that are difficult to measure. This chapter discusses the necessity for atomic structure calculations and the motivation of using alkaline-earth atoms such as Sr for these purposes.

One of the strongest reasons for theoretical calculations comes about because of the desire to understand the basic quantum mechanical behavior of atoms. Interpreting experimental data such as energy state lifetimes and dispersion coefficients of molecular potentials requires high-precision computations of the atomic structure because theoretical calculations can guide experiments toward sound conclusions. Sometimes measurements require a guideline when there is disagreement within the values. Porsev et al. comment on this situation in the case of the value for the tran-

sition oscillator strengths and lifetimes for the $^3P_1$ state for magnesium, calcium and strontium, where discrepancies between experimental and theoretical values still exist [12]. When the theory is checked and refined such that all important correlations are correctly accounted for, it can be trusted for other types of quantities, such as ac Stark shifts and excited state linewidths.

The complexity of the alkaline-earth metal system challenges both current theory and the process by which the calculations are brought about. Current theory used for treating two valence electron, like in the case of alkaline-earth metal atoms and Yb, has developed after realizing the different correlations that are important in such systems. The investigations began with nonrelativistic methods, but soon began to include relativistic contributions that accounted for the intravalence correlations [32]. Also, core-valence interactions were included through core-polarization corrections [32] and, more recently, through many-body perturbation theory (see, for example, [13]). Different schemes to improve the accuracy and timing of calculations are also developed through work with alkaline-earth metal systems. Some of these schemes include energy minimization of the initial and final states [32, 33] and use of more efficient basis sets such as Slater basis sets [34].

Theoretical investigations using Sr have been active for many years, as seen in the references found in Chapter 5. It is also necessary to compare calculations to measurements to validate the theory. To this end, the following chapters introduce

the experimental method and results from the lifetime measurement performed here, and then compare it to more recent theoretical values available.

Chapter 3
Electron Shelving technique

To measure the lifetime of the $^3P_1$ state, it is necessary to excite atoms to the state and to measure the rate at which those atoms decay out of the state. This chapter introduces the history and theory behind electron shelving, the measurement method used to perform the lifetime measurement. It also contains a discussion of the absorption image analysis performed for the measurement.

3.1 Naive Experimental Setup

In order to study the $^1S_0 \rightarrow {}^3P_1$ transition, it might appear straightforward to simply excite the transition under some set of conditions and collect the scattered photons of this transition. This procedure is depicted in Figure 3.1. However, since the photon scattering rate is proportional to the linewidth of the transition, the maximum number of photons scattered off of this transition per second is on the order of 10^3 photons. Only a fraction of these fluorescence photons are collected, producing a small signal. Separating this signal from the noise level of the experiment becomes difficult. Although it can be done with single-photon counters (for example, see Ritter and Eichmann [35]), a different monitoring method might be better.

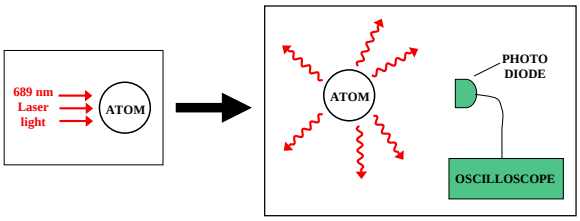

Figure 3.1 This diagram depicts a straightforward approach to studying the ${}^1S_0 \rightarrow {}^3P_1$ transition dynamics. A 689 nm laser beam falls on an atom and the atom scatters photons. The fluorescence of this experiment is collected, which results in a small signal due to the low scattering rate of this transition. Even though this type of signal monitoring is possible, using electron shelving can magnify the fluorescence signal to facilitate an accurate measurement.

3.2 Idea of the Electron Shelving Technique

To overcome the difficulty of the previous experiment, consider the following technique. Sr has an energy level system composed of two excited states labelled ${}^1P_1$ and ${}^3P_1$, both coupled to the ${}^1S_0$ ground state as shown in Figure 3.2. The ${}^1P_1$ state has a large spontaneous decay rate of Γ_1, typical of an E1 transition to the ${}^1S_0$ state. The ${}^3P_1$ state has a much smaller decay rate of Γ_2, typical of an intercombination line transition.

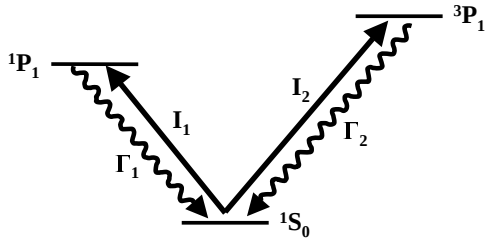

Figure 3.2 A simplified energy level diagram of Sr with transitions of very different rates. The ${}^1P_1$ state has a typical E1 transition rate Γ_1, while the ${}^3P_1$ has a small transition rate Γ_2 compared to Γ_1. When I_2 is applied to an ensemble of these atoms, some of them are excited to the ${}^3P_1$ state, and then slowly decay back to the ${}^1S_0$ state. During this time, information about the repopulation of the ground state due to atoms returning from the ${}^3P_1$ state can be monitored through the ${}^1S_0 \rightarrow {}^1P_1$ transition.

If laser light of intensity I_1 and resonant with the $^1S_0 \rightarrow {}^1P_1$ transition is applied to an ensemble of these atoms, the amount of scattered light measured is proportional to the number of atoms initially in the $^1S_0$ state. Atoms in the $^3P_1$ state will not be counted. Now, if I_2 excites atoms to the $^3P_1$ state, they will slowly decay back to the ground state because of their small decay rate Γ_2. If I_1 is then applied to the ensemble of atoms while a certain population of atoms occupy the $^3P_1$ state, the amount of scattered light will be a measure of only those atoms left in the $^1S_0$ state. Therefore, the number of atoms in the $^3P_1$ state can be measured dynamically without direct interaction with the $^3P_1$ state by turning on I_1 and observing the amount of light scattered off of the $^1S_0 \rightarrow {}^1P_1$ transition. This simple idea is behind the electron shelving technique, the main tool used in the experiments for these lifetime measurements.

It is worth emphasizing that this technique allows the energy state in question to decay naturally. By shelving the atoms to the $^3P_1$ state and probing the $^1S_0 \rightarrow {}^1P_1$, the $^3P_1$ population is unperturbed by the 689 nm laser used to excite the atoms, therefore providing a more accurate lifetime measurement. Also, the signal of the $^1S_0 \rightarrow {}^3P_1$ transition is greatly enhanced by probing the broader transition. The larger linewidth of the broad transition (on the order of tens of MHz) supports about 10^3 times more photon scattering when compared to the intercombination transition for Sr.

3.3 Absorption Method

For this lifetime measurement, the absorption was measured instead of the fluorescence, but the idea is the same; this is because the "absorbed" light corresponds to the photons that are scattered. When the absorption of an incident laser beam from an atom cloud is monitored, for instance, the signal falling on the measurement device is related to the number of photons missing from the incident beam because of the atom cloud. In this lifetime experiment, the transmitted laser beam falls on a camera and is recorded as an absorption image. The experimental procedure for taking images of the atom clouds is discussed in Chapter 4. Here the image diagnostics used to measure the number of $^1S_0$ state atoms are discussed.

The relationship between the incident and transmitted laser beam signals is defined by the following equation:

$$I_{trans} = I_{inc} e^{[-OD(x,y)]}, \tag{3.1}$$

where the optical depth $OD(x, y)$ is related to the density of the atom cloud by

$$OD(x, y) = \int_{-\infty}^{\infty} n(x, y, z)\alpha_{abs}\,\mathrm{dz}. \tag{3.2}$$

Here, $n(x, y, z)$ is the distribution function for the number density in the MOT and α_{abs} is the photon absorption cross section of the atoms. The expression for α_{sat} is

$$\alpha_{abs} = \frac{3\lambda^2}{2\pi} \frac{1}{1 + (I/I_{sat}) + (2\Delta/\gamma)^2}. \tag{3.3}$$

The detuning of the image beam from the atomic resonance is Δ, while the linewidth of the transition is specified by γ. I is the intensity of the incident laser, and I_{sat} is the saturation intensity of the atomic transition driven by the incident laser.

The intensity of the incident light is determined by taking a background absorption image of the signal falling on the camera without an atom cloud in the path of the image laser beam. Then a measurement is made with an atom cloud to create an absorption image. From both the background and absorption images, the OD of the sample can be determined by using the following equation

$$OD(x, y) = ln[I_{inc}(x, y)/I_{trans}(x, y)]. \tag{3.4}$$

Figure 3.3 shows a typical absorption image.

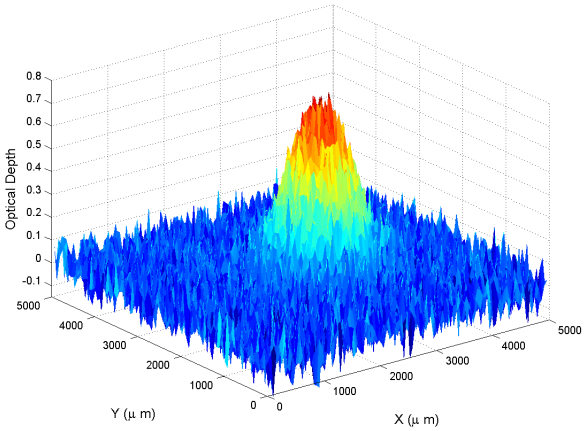

Figure 3.3 A sample absorption image, showing the OD of an atom sample.

Many characteristics of the atom cloud, such as cloud size and temperature, can be derived from these absorption images. The number of atoms in the cloud is probably the most important value for the lifetime measurements that is extracted from the

absorption images. Two methods were used to determine the number of atoms in the $^1S_0$ state.

In the first method, the OD was numerically integrated over a specific area of the camera that included the entire cloud shadow. Then, the number of atoms was related to the OD through Equation 3.2 and obtained from the ratio

$$N_{OD} = \frac{\int\int OD(x,y)\,\mathrm{dx}\,\mathrm{dy}}{\alpha_{abs}} \tag{3.5}$$

where α_{abs} is determined through Equation 3.3.

The second method used to obtain number-of-atom information was through a fit of the data. If the density distribution is Gaussian, Equation 3.2 implies

$$OD = \frac{\alpha_{abs} N_{Gaussian}}{2\pi\sigma_x\sigma_y} exp\left[-\frac{x^2}{2\sigma_x^2} - \frac{y^2}{2\sigma_y^2}\right]. \tag{3.6}$$

A fit to the OD yields $N_{Gaussian}$.

These two methods were employed because one method may be more correct than the other under certain circumstances. If the absorption image taken during a measurement were to have fallen off of the camera, then the numerical integration of the OD would not be able to give the correct number of atoms, while the Gaussian fit function would still be able to fit the image reasonably to give a correct atom count. If, on the other hand, the absorption image of the measurement was impaired due to an excessive background slope or offset, or the density does not follow a Gaussian, then the performance of the numerical integration in determining the number of atoms

would be superior to that of the Gaussian fit. A comparison between the number of atoms computed through both methods shows that they agree, as seen in Figure 3.4.

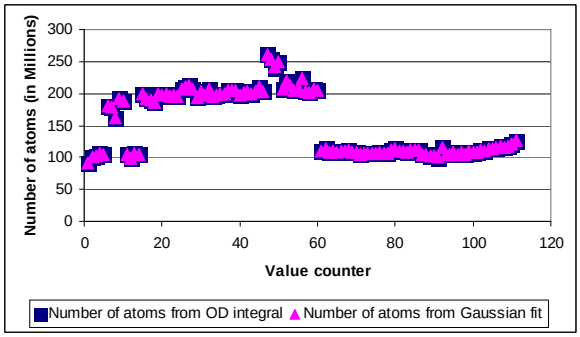

Figure 3.4 This plot shows the atom count obtained through 1) numerical integration of OD signal over a specific camera size and 2) Gaussian fit parameters. The compatibility of the data ensures that both procedures give the same atom population and that the data signals are above noise levels.

3.4 Background of the ES Technique

The "shelved optical electron" atomic amplification scheme, also known as "electron-shelving" or simply "shelving", was first proposed by Dehmelt in 1975 [1] and experimentally realized not long after that. In 1986, Nagourney et al. demonstrated the shelving of an individual barium ion in the optical metastable $5^2D_{5/2}$ level with a lifetime greater than 30 seconds [36]. A similar experiment was performed before Nagourney et al. using microwave-optical transitions in an ion cloud [37]. The first theoretical treatment of the shelving technique was presented by Cook and Kimble [38] in 1985. Since then, the shelving technique has been widely used in atomic physics, including in ion experiments (see for example Wineland et al. [37] and Knoop et al. [39]), for high resolution spectroscopy of atoms (Oates et al. [23] and Takamoto

and Katori [26]), and to measure lifetimes and radiative rates of metastable states (Itano et al. [40] and Yasuda and Katori [41]). Researchers have also explored the underlying theory of the process (see, for example, Blatt and Zoller [42]).

Chapter 4
Lifetime Measurements

As seen in the last chapter, electron shelving can facilitate the study of the $^1S_0 \rightarrow {}^3P_1$ transition. An important parameter to study is the lifetime of an atomic state. In this chapter, the experimental procedure followed to obtain the lifetime measurement is presented.

4.1 Experimental Procedure

The lifetime measurement begins with a 461 nm magneto-optical trap (MOT), obtained through well-known laser cooling and trapping procedures [43]. Figure 4.1 shows a schematic drawing of the blue MOT experimental setup. The $^1S_0 \rightarrow {}^1P_1$ transition is used for this first-stage cooling, and it provides atom samples with temperatures of a few mK and Gaussian density profiles of around 6×10^9 cm^{-3}. The number of atoms initially in this blue MOT cloud is typically $4-5 \times 10^8$ with a cloud radius of 1.5 mm. These atoms are then transferred into a 689 nm MOT for 300 ms of cooling time, resulting in a MOT temperature of $4-10$ μK and densities between 2 and 3×10^{10} cm^{-3}. The setup for the red MOT is very similar to the blue MOT seen in Figure 4.1. Red MOT beams are sent to the trapping apparatus through an acousto-optic modulator (AOM). The number of atoms in the red MOT cloud before the lifetime measurements range from $1-2 \times 10^8$, and the clouds typically have radii

of 0.5 mm. Adjusting magnetic fields and ramping the laser power during the cooling stage allows us to modify the red MOT characteristics.

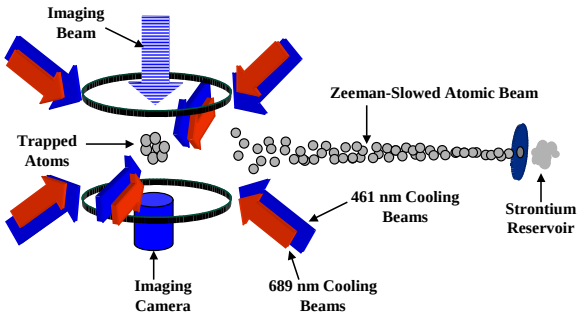

Figure 4.1 The experimental setup for lifetime measurements described in this chapter is shown. Sr atoms from vapor obtained by heating solid Sr held in a reservoir are slowed by a Zeeman laser beam (not shown). The atoms enter a region of magnetic fields and six counter-propagating laser cooling beams. Two-stage cooling occurs (blue and red MOT cooling) and lifetime measurements are made by applying the image beam on the atoms. The atoms cast a shadow on the CCD camera. Adapted from [44].

When the atomic sample has equilibrated in the red MOT, the atoms are subject to a delay time τ_d, during which all magnets and laser beams are turned off (see Figure 4.2 showing the timing sequence followed). Time τ_d was chosen to allow the cloud to expand for a particular image beam detuning so the OD of the atom cloud was low enough to get a good measurement of the number of atoms (see Section 3.3 for an explanation of the relationship between the atom count and the OD). For the most part, τ_d was 30 ms, but it was also chosen to be 5 ms when the image beam frequency was far-detuned. Section 5.1 discusses the image beam detuning and delay times used in the lifetime measurements. If this delay time were to be applied after the interaction of the atoms with the pump beam, the dynamics of the population

evolution would not be seen. Also, if this delay time was chosen to be larger than about 30 ms, the atoms would fall out of the viewing area because of gravity.

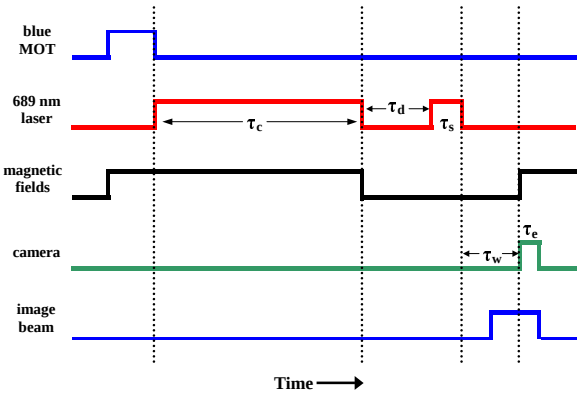

Figure 4.2 The timing sequence for the lifetime experiment is shown. A high signal implies that the particular experimental component is turned on; a low signal signifies that it is off. Blue MOT cooling occurs first. Then red MOT cooling occurs for a time τ_c, after which everything is turned off for a delay time τ_d. The 689 nm laser beams are turned on for an interaction time τ_s and the atoms populate the $^3P_1$ state. The waiting time τ_w is varied between 5 and 104 μs to reveal the dynamics of $^1S_0$ repopulation from $^3P_1$ state atoms. The camera is exposed for a time τ_e. This timing sequence is followed for every lifetime measurement made. Note that the image beam is turned on before a camera image is taken. This is done to account for the response time of the AOM supplying the image beam.

After this waiting time, the 689 nm beams were turned on once more for a specific amount of interaction time τ_s, during which the laser beam's frequency was at the $^1S_0 \rightarrow {}^3P_1$ transition frequency. τ_s took on values of 200 and 500 μs. Applying the 689 nm laser at the resonance frequency excites atoms in the ground state to the $^3P_1$ state. The length of τ_s is on the order of 100 μs to insure a steady state population in the $^3P_1$ state on the order of 50% of the total number of atoms. The procedure to choose the resonance frequency for the 689 nm laser is discussed in Section 4.2.

After the 689 nm beams interact with the atomic sample for the time τ_s, another waiting time τ_w is introduced. This waiting time is varied between 5 and 104 μs, allowing the $^3P_1$ population to decay to the $^1S_0$ state. A collimated image beam much larger than the atom sample and tuned near resonance with the 461 nm transition is then applied onto the atoms with an AOM. The atoms scatter photons and cast a shadow onto an image-intensified CCD camera. The resulting absorption image is analyzed to extract the OD and the number of atoms in the $^1S_0$ state. Section 3.3 described in detail how the number of atoms is determined from these images.

A few comments need to be made at this point. The camera gate width time for all of the absorption images is 2 μs. A short gate width was chosen because the dynamics of the system evolve within 100 μs. Also, note that delays shorter than 4 μs were not taken during a lifetime measurement to allow the 689 nm beam AOM to turn off and the 461 nm image beam AOM to turn on. Finally, the image beam detuning from the $^1S_0 \rightarrow {}^3P_1$ state was changed judiciously, along with the delay time τ_d, in order to provide different optical depths for systematic reasons. About 50% of the data was taken with an image beam detuned 23 MHz to the red of the $^1S_0 \rightarrow {}^3P_1$ transition frequency. τ_d for this detuning was 30 ms. Another 25% of the data was taken with a τ_d of 5 ms and an image beam detuned 49 MHz to the red of the transition frequency. The remaining 25% of the measurements were taken with the image beam red detuned to 34 MHz and a τ_d of 30 ms. The resulting optical depths

due to these experimental conditions are discussed in Chapter 5.

Having determined the number of atoms in the atom cloud and knowing the delay time before camera exposure, the repopulation of the $^1S_0$ state is plotted, such as in Figure 4.3. These lifetime curves are fit to

$$N(t) = N_0[1 - Ae^{(-\frac{t}{\tau})}], \tag{4.1}$$

where N_0 is the number of atoms in the ground state before excitation to the $^3P_1$ state by the 689 nm laser, A is the amplitude of the repopulation curve, and τ is the measured lifetime of the $^3P_1$ state. The entire experimental procedure described above was repeated for 111 profiles. All the timing in the experiment has 10 ns resolution.

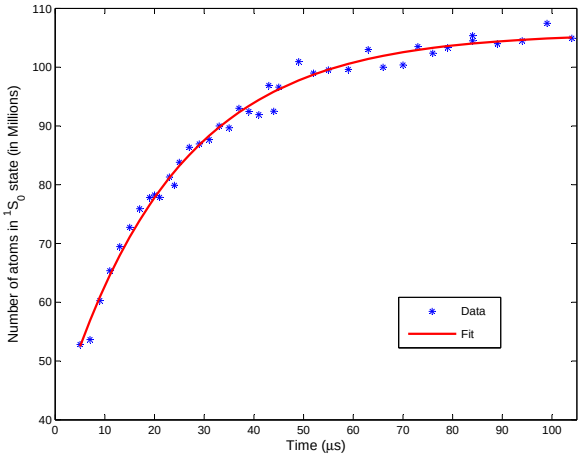

Figure 4.3 A sample lifetime measurement, showing the fit curve used to obtain the lifetime value. This repopulation curve corresponds to a lifetime value of 23.4 μs.

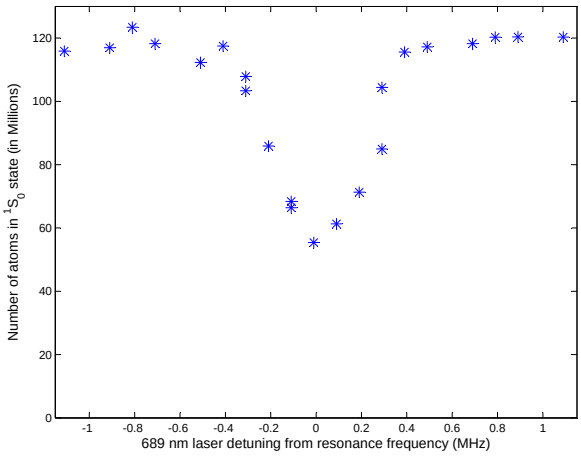

Figure 4.4 The resonance frequency used for the 689 nm laser during the lifetime measurements is obtained from these spectrum curves. The laser frequency that depletes the $^1S_0$ population maximally is used for the resonance frequency.

4.2 Determining the Resonance Frequency

To obtain the maximum initial population difference for the $^1S_0$ state, the 689 nm laser frequency during τ_s was chosen to be the resonance frequency of the $^1S_0 \rightarrow {}^3P_1$ transition. As stated previously, the 689 nm laser is controlled by an AOM whose supply voltage is controlled by an experimental computer. The resonance frequency was obtained by taking a spectrum of the absorption of the atoms as they interacted with the 689 nm laser (see Figure 4.4).

In order to determine this resonant frequency, the following procedure was followed. An atomic cloud is cooled as described above in the blue and red MOTs. After MOT cooling, the delay time τ_d is waited (usually chosen to be 30 ms) during which all magnetic fields and laser beams are switched off. After τ_d, the 689 nm laser is turned on again and interacts with the atoms as its frequency is stepped about 100

kHz per data point. τ_s here is also on the order of 100 μs as before. After τ_s, the 461 nm image beam is turned on, and an absorption image is taken to measure the percent of atoms removed from the $^1S_0$ state by the 689 nm laser. The frequency of the 689 nm beam that caused the maximal amount of loss in the number of atoms in the ground state is the resonance frequency of the $^1S_0 \rightarrow {}^3P_1$ transition. Then the 689 nm laser frequency can be tuned to this resonance frequency, and the lifetime experiment follows the description given above.

Unfortunately, there was a slow drift of the frequency during the course of the data taking, which became noticeable by the drop in the initial population difference for the $^1S_0$ state. As the drift became apparent, the frequency of the AOM was shifted to compensate for the loss of absorption signal. The drift was no larger than 60 kHz/hr. A discussion on this laser drift and its possible effects on the data is found in Chapter 5.

Chapter 5
Discussion and Conclusion

Analyzing the lifetime data taken for this thesis has uncovered problems and has taught many lessons. The results of the lifetime measurements are shown in Figure 5.1. This figure consists of 111 lifetime measurements taken on three different days. The mean value for the lifetime of the $^3P_1$ state is 22.6 μs with a root-mean-square deviation of 3.4 μs, giving a statistical uncertainty of 0.3 μs. However, a systematic deviation is noticeable in the data from the third day's measurements, and the systematic uncertainty of the experiment is the dominant contribution to the overall uncertainty (see Figure 5.1).

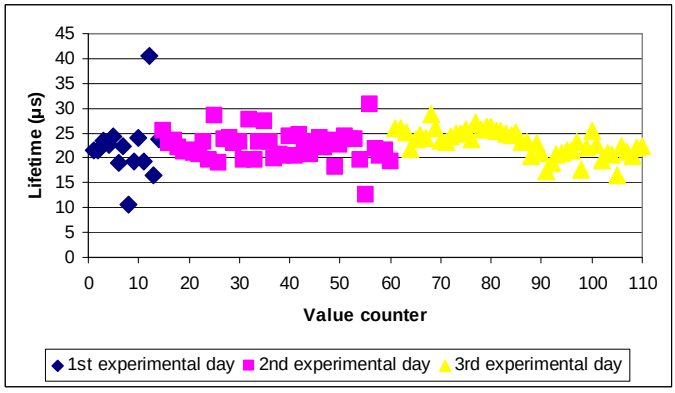

Figure 5.1 A compilation of the lifetime values from fits of repopulation curves for all of the experimental days. Data from the first experimental day is not as reliable as the other data sets. There are a total of 111 points in this compilation. The value counter is just an index labelling the profiles.

If the lifetime measurement is identified with its corresponding image beam detuning, the plot of lifetime values would look like Figure 5.2. There is a noticeable step

in the lifetime values at image beam detunings of 34 MHz and 49 MHz. It is interesting to analyze each region of data separately according to the image beam detuning. Region A is comprised of 60 data points and gives a mean lifetime value of 22.3 μs, with a standard deviation of 4.0 μs and a statistical uncertainty of 0.5 μs. Region B has 26 data points, and its mean lifetime is 25.0 μs with a standard deviation of 1.4 μs and 0.3 μs for the statistical uncertainty. Finally, region C contains 25 data points and gives a mean lifetime value of 21.1 μs, with a 1.9 μs standard deviation and a statistical uncertainty of 0.4 μs. The three regions give lifetime values that do not agree with each other within their statistical uncertainties.

The experimental conditions were varied to test for systematics, and unfortunately, a systematic error is noticeable in the data. The following sections will discuss the possible sources of the systematic deviation and the implication for the lifetime measurement.

5.1 Optical Depth Considerations

Systematic uncertainty is a major concern during the experiment because it is difficult to remove and account for. One of the most important experimental uncertainties to minimize comes from correctly counting the atomic population in the $^1S_0$ state. The population counting is directly related to the OD of the sample; it is vital to make sure that the sample is not too optically thick in the imaging transition ($^1S_0 \rightarrow {}^1P_1$). If an optically thick sample is imaged, very few photons reach the

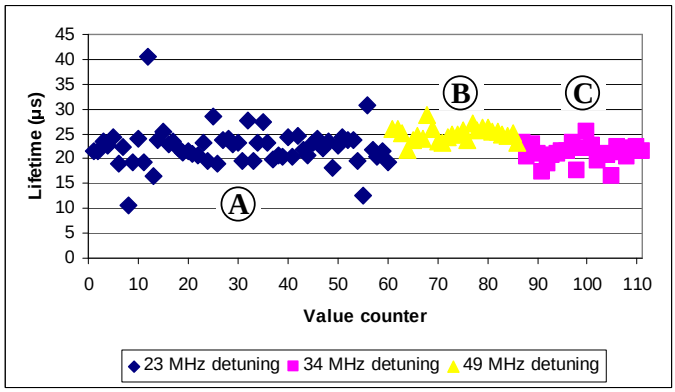

Figure 5.2 The lifetimes are plotted while distinguishing between the three different image beam detunings used in the experiment. The "step" seen between regions B and C signals that there is a systematic error in the experiment. All experimental conditions between these two data sets are the same except for image beam frequency and delay time τ_d.

camera, and the result is a signal sensitive to the background level or to sources of noise. When the OD is too thick, the relationship between the incident and transmitted laser intensities, as stated in Equation 3.1, is not true anymore because the background level is not removed from either the incident or transmitted signals in this experiment. Furthermore, the atom count at high OD values is lower than it should be; this situation would lead to a shorter lifetime for that measurement.

The image beam detuning was changed three times during the lifetime measurements. These three experimental conditions give different OD values. For the 23 MHz detuning and delay time of 30 ms, the peak OD has values between 0.5 and 1.15. Under these conditions, few lifetime data points were taken with a population of about 1×10^8 atoms, and the rest of the lifetime data points were taken with about 2×10^8 atoms. An image beam detuning of 49 MHz and a delay time of 5 ms gives

OD values of about 0.8. The atom population during these measurements was about 1×10^8 atoms. For the 34 MHz detuning and delay time of 30 ms, the OD value is about 0.5. This data was taken with an atom population of about 1×10^8 atoms.

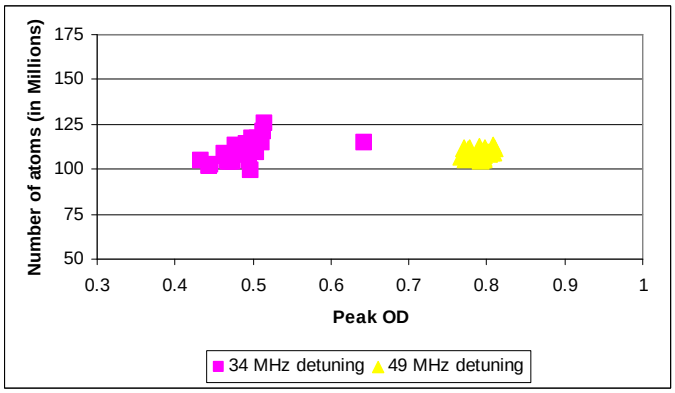

Figure 5.3 The number of atoms versus peak OD with image beam detuning indicated. The same number of atoms for both frequency detunings is expected because the trapping part of the sequence is the same for all of the data. This behavior is seen in this figure, indicating the counting of atoms is not sensitive for OD less than or equal to 0.8.

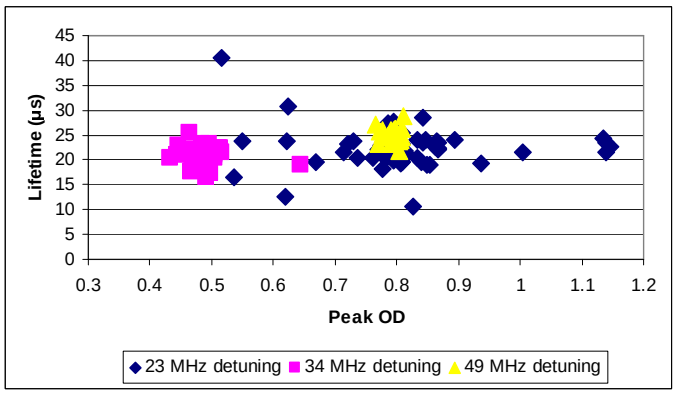

Figure 5.4 Plot of the lifetime values versus peak OD with image beam detuning indicated. This plot shows that for the most part, the value of the OD of the atom samples is reasonable. The lifetime values at optical depths between 1.0 and 1.15 correspond to some of the first experimental day's data points.

When the OD is reasonable, the number of atoms is correctly counted. This can

be seen in Figure 5.3, where the number of atoms for image beam detunings of 34 MHz and 49 MHz are the same even though the OD for the 34 MHz detuning is about half that of the OD for the 49 MHz detuning. The data for 34 MHz and 49 MHz detunings is only differentiated by the frequency of the image beam and the delay time used for the measurements. Therefore, experimentally, these two detunings have the same number of atoms. The analysis also agrees with this conclusion.

There are a few lifetime data points, with OD values between 1 and 1.15 for data taken with the image beam detuned to 23 MHz, which could be suspect when considering the correct atom count (see Figure 5.4). However, the data obtained with an image beam detuning of 23 MHz is also noisy, and in general, it is not as reliable as data taken at the other image beam detunings. Data taken at the 34 MHz and 49 MHz detunings is a lot quieter than of the 23 MHz detuning. High noise levels are mostly due to the laser locks not being optimized. Nevertheless, the optical depths of the atom samples for most of the data is in a safe range between 0.35 and 0.9. Therefore, the optical depths give the correct number of atoms, which implies that the OD does not contribute significantly to the systematic error observed.

5.2 Laser Drift Considerations

As stated in Section 4.2, the frequency of the 689 nm laser drifted during the lifetime measurements; the drift was measured to be no more than 60 kHz/hr. This drift raises concerns about the stability of the number of atoms during the time that

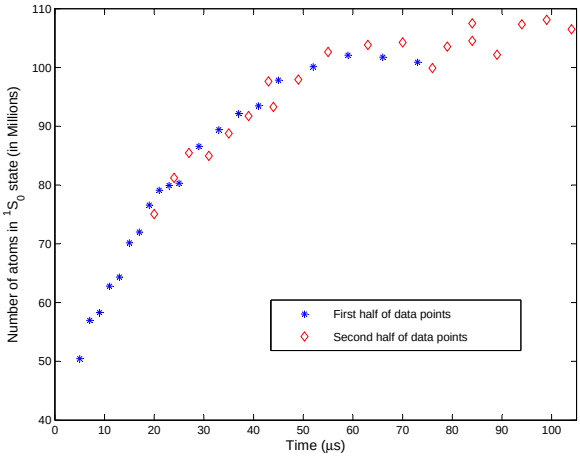

Figure 5.5 A lifetime curve with the time elapsed between data points differentiated. The first half and second half of the data set is distinguished to show that the laser frequency drift experienced by the 689 nm laser does not affect the lifetime curve.

data points are acquired for a lifetime decay curve. Since the drift of the laser results in a change of population excited to the $^3P_1$ state, then one experimental decay curve, which could take as long as 10 minutes, could be affected by this drift.

However, Figure 5.5 shows that the laser drift does not actually affect the data. This figure shows a lifetime curve composed of 40 individual data points, distinguished by the time in which they were taken. If the laser drift was in fact a problem, then a noticeable separation between the first half and the second half of the data points would exist. The laser drift would cause a difference in the number of atoms counted in the first half of the data points in comparison to the second half of the data points. Therefore, as seen in Figure 5.5, the laser drift does not contribute to the systematic error observed.

5.3 Other Observations

Other possible sources of error need to be addressed to account for the systematic error seen in the data, since the OD values for the lifetime measurements and the laser frequency drift do not account for it. One possibility involves atoms leaving the imaging region. In some experiments, atoms leaving the region of observation may seem like atom population loss. This loss might affect the lifetime measurement by introducing an extra decay factor for the initial population in Equation 4.1. However, at temperatures on the order of 10 μK, the velocity of the Sr atoms is around 4.4 cm s^{-1}. The Sr atoms do not travel much at all after 100 μs, so it is improbable that they have left the imaging region. In the presence of gravity, the atom cloud can fall about 50 nm in 100 μs, a length short enough that these atoms have not left the observation region. Therefore, this effect is negligible.

Collisions between Sr atoms and background atoms can contribute to the loss of atoms from the observation region. Therefore, it is necessary to determine the size of this effect by estimating the rate at which it occurs. The base pressure of the experimental chamber is below $P = 6 \times 10^{-9}$ mbarr, as measured by the ion pump current. This pressure corresponds to a collision rate, per Sr atom with the background atoms, of $\gamma_{bg} \simeq n_B \sigma_{bg} v_{bg} = 0.06$ s^{-1}, where n_B is the density of background atoms in the chamber and $v_{bg} \simeq \sqrt{\frac{2kT}{M}}$ is the relative velocity between the Sr and N_2 atoms at room temperature. σ_{bg} is typically on the order of 10^{-14} cm^2 for Sr collisions with a

foreign gas [45]. The collision time turns out to be on the order of ten seconds. This estimated time is reasonable when compared to a previous experiment with magnetically trapped Sr atoms in the $^3P_2$ level [43]. The magnetic trap lifetime was on the order of 1 second and was limited by background collisions. Since the dynamics of the lifetime experiment occurs within 100 μs of an atom's excitation to the $^3P_1$ state, the time scale at which these collisions occur is much longer than those important to the lifetime measurement.

A similar rate for collisions between Sr atoms in the cloud should also be considered. These collisions could have the effect of decreasing the natural lifetime of the state [39]. The cross section for collisions between Sr atoms, from Crane et al. [45], has a measured value of $\sigma_{Sr} = 6.55 \times 10^{-14}$ cm^2. This value corresponds to a rate $\gamma_{2body} \simeq n_{Sr}\sigma_{Sr}v_{Sr} = 5.7 \times 10^{-3}$ s^{-1}, where $n_{Sr} = 2 \times 10^{10}$ cm^{-3} is the density of the Sr cloud, and $v_{Sr} \simeq \sqrt{\frac{2kT}{M}}$ is the average velocity between colliding atoms at $T = 10\mu$K. This time scale is also much longer than the dynamics of the lifetime measurement.

Another potential concern involves the possibility of optically pumping population to the $^1D_2$ state by the image probe beam. The $^1S_0 \rightarrow {}^1P_1$ transition is not exactly a cycling transition, and atoms excited to the $^1P_1$ state can decay to the $^1D_2$ state, perturbing the count of ground state atoms. However, the loss of atoms to the $^1D_2$ state does not affect the measured lifetime; even if optical pumping to the $^1D_2$ state was appreciable, this effect would only reduce the signal being measured. The

branching ratio of the decay to the $^1D_2$ state is $\Gamma_{^1P_1-^1D_2}/(\Gamma_{^1P_1-^1D_2} + \Gamma_{^1P_1-^1S_0}) \simeq 1.9 \times 10^{-5}$ [17, 46]. The number of photons scattered per atom, during the 6 μs time the image beam is on, is about 60, which corresponds to a probability of 10^{-3} for an atom to decay to the $^1D_2$ state. Therefore, the loss of atoms to the $^1D_2$ state due to the image beam is also negligible.

The most appealing explanation to account for the systematic error involves the alignment of the imaging beam. Since the detuning of the image beam is changed through an AOM, the alignment of the beam needs to be adjusted for each detuning. As the image beam is realigned, there can always be some portion of the zeroth order beam scattered off of the atoms if the alignment is not satisfactory. 461 nm light scatters off atoms very efficiently and may affect the lifetime measurement. This extra signal may account for the systematic error in the data. Further investigation is required in order to attribute the systematic error to poor beam alignment. However, the other obvious possibilities do not seem to contribute significantly enough to the error in the data.

5.4 Discussion of Measurement

As stated above, the lifetime data collected in the experiment gives a lifetime value for each of the three image beam detunings. These three values do not agree with each other. A consideration of possible experimental errors does not seem to explain the systematic uncertainty seen in the data. Planned future work will need

to include better stability of the experiment and additional lifetime measurements to rectify these results.

The statistical uncertainty ranges of the three different regions implies that a precision on the order of 0.1 μs is possible if the systematic error is reduced. This lifetime measurement is limited by systematic uncertainty, but we give 23$\pm$3 μs as our best estimate.

5.5 Comparison with Literature

Experimental measurements of the lifetime or oscillator strengths have been done using various experimental techniques such as interferometric methods [9], atomic beam techniques [10], and time-resolved emission or absorption measurements following dye-laser excitation [11, 47–51]. A useful compilation of mean lifetime values before 1983 can be found in Husain and Schifino [47]. These values range from 6.4 to 74 μs.

Recent experiments have concentrated their efforts on lifetime measurements using emission or absorption monitoring after laser excitation of Sr. These experimental values are tabulated in Table 5.1. The basic idea is the same for all of the experiments: Sr vapor in the presence of a buffer gas is excited by a pulsed dye-laser at $\lambda = 689.45$ nm, and the fluorescence is monitored by a photomultiplier, revealing a decay of the excited $^3P_1$ atoms. Borisov et al. uses absorption monitoring instead of emission [48]. Drozdowski et al. uses an atomic beam of Sr instead of Sr vapor [11].

^{88}Sr $^3P_1$ State Lifetime Values

Type	Ref.	Value	Year
Experiment	[47]	20.1 ± 0.4 μs	1984
Experiment	[48]	20.9 ± 0.9 μs	1985
Experiment	[49]	19.1 ± 0.4 μs	1985
Experiment	[50]	$19.6^{+0.6}_{-0.5}$ μs	1988
Experiment	[51]	22 ± 0.5 μs	1988
Experiment	[11]	21.3 ± 0.5 μs	1997
This work		$\mathbf{22.64 \pm 3}$ **μs**	**2005**
Theory	[34]	21.2 μs	1984
Theory	[33]	39.96 μs	1984
Theory	[32]	16.7 μs	1987
Theory	[52]	15.7 μs	1993
Theory	[12]	18.72 ± 0.372 μs	2000
Theory	[13]	18.96 ± 0.356 μs	2001
Theory	[14]	18.04 μs	2002
Theory	[15]	24.4 ± 2.4 μs	2004

Table 5.1 Compilation of current experimental and theoretical values.

There is a large spread in the various measured lifetime values, and when considering their stated uncertainties, the values do not really overlap. Based on the measurements in the table, the lifetime of the $^3P_1$ state is between 19 and 22 μs. Our experimental value of 23 μs, even neglecting concerns about systematic errors, is the highest experimental value, as seen in Table 5.1. However, our experiment is also the first to use laser-cooled atoms to measure the lifetime of the $^3P_1$ state. The measurement performed by Kelly et al. [51] is the closest experimental value to our value. It is interesting to note that our lifetime measurement yields a higher lifetime than values measured by other experimental procedures because, as noted, most systematic errors decrease the measured lifetime [39]. A larger measured lifetime suggests that our

experimental procedure might be less susceptible to situations limiting the lifetime of the $^3P_1$ state. These situations may include frequent collisions with a buffer gas and the loss of higher velocity atoms from the measuring region. The largest uncertainty in previously published measurements is less than 1 μs.

Theoretical values found in the literature were computed using different methods to incorporate necessary correlations such as intravalence and core-valence electron interactions. Multiconfiguration Hartree-Fock (MCHF) [32], multiconfiguration Dirac-Fock (MCDF) [32, 33], and configuration interaction (CI) theory [12–14, 32] have been used to treat valence-valence electron correlations. Interactions between core and valence electrons were treated using core-polarization [32] corrections and many-body perturbation theory (MBPT) [12–14]. Santra et al. solves the two valence electron Schrödinger equation with a potential that models the ionic core [15].

Calculations performed by theorists include oscillator strengths (or f-value), and in order to convert to a lifetime value, the following equation was used [53]:

$$\tau = \frac{mc\epsilon_0}{2\pi e^2 f}\frac{g_2}{g_1}\lambda^2. \tag{5.1}$$

$\lambda = 689.45$ nm is the wavelength used for the conversion. $g_1 = 1$ and $g_2 = 3$ are the degeneracies of the $^1S_0$ and $^3P_1$ energy states, respectively. Sometimes, reduced matrix elements were tabulated, and a conversion from the matrix element to a transition

rate coefficient is made through the following equation [13]:

$$A_{FI} = \frac{2.02613 \times 10^{18}}{\lambda^3} \frac{|\langle F \| D \| I \rangle|^2}{(2J_I + 1)}. \tag{5.2}$$

Here, D is the dipole operator and $J_I = 1$ is the total angular momentum quantum number of the $^1S_0$ state. Transition rates were converted to lifetimes through the relation $\tau = 1/A$, where A is the transition rate. The length gauge value of the oscillator strength or reduced matrix element was chosen instead of the velocity gauge because the velocity gauge seems to be more sensitive to many-body corrections than the length gauge [13].

Current theoretical values have a much larger spread than the measurements in the literature, as seen in Table 5.1. Most of these values are much lower than our measurement of 22.64 μs. The value from Santra et al. [15] is the closest theoretical value to our measurement. It is interesting to note that this calculation suggests a higher lifetime than values from current measurements. The large spread in the calculated lifetime values confirms the fact that current theory needs a more accurate lifetime measurement to compare to.

In conclusion, given the fact that the lifetime measurements performed suffer from systematic error, this experimental procedure has not yet provided a more accurate value for the lifetime of the $^3P_1$ state. As it is, our data suggests a lifetime value of 23$\pm$3 μs. Despite the large systematic error we observe, our method may still be useful as evidenced by our small statistical uncertainty. In order to improve the

accuracy and precision of this lifetime measurement, more care should be taken to remove systematic errors and to ensure laser stability. Another important addition to the experiment would be real time data analysis so that the analysis can guide the experiment and problems can be explored quickly. With a more careful analysis and control of the systematic errors, we can make a significant contribution to the understanding of the $^3P_1$ energy level.

Appendix A
Lineshape Studies of the $^1S_0 \rightarrow {}^3P_1$ Transition

Because the lineshape of the $^1S_0 \rightarrow {}^3P_1$ transition is so narrow, it is very sensitive to many different effects. A couple of these effects were studied and are presented in this appendix. These three lineshape studies are useful to zero any external field influence on the atomic clouds. They also help to place an upper limit on the laser linewidth.

Because the interaction time (on the order of 100 μs) for the atoms with the 689 nm laser is much longer than the coherence time of the laser, Rabi oscillations of the population between the ground and excited states are not a concern. The coherence time of the laser is about $\Delta t = 1/2\pi\Delta f \sim 1.6$ μs, where $\Delta f = 100$ kHz is the linewidth of the 689 nm laser.

The experimental procedure for these lineshape studies is mostly described in Chapter 4, with a few changes depending on the particular study. Sr atoms subject to the different effects presented here were pre-cooled through the two-stage cooling. The atoms are then allowed to expand for an expansion time τ_d. Next, the atoms interact with the 689 nm laser for an interaction time τ_s. Another delay time τ_w is introduced before an absorption image of the atom cloud is taken. Whenever the timing or the experimental procedure for the study being discussed is different than

that described in Chapter 4, the difference is defined in the specific section.

A.1 Magnetic Field Effect

The effect of an external magnetic field on the red MOT was observed by varying the field and taking absorption images of the atoms. Transitions tune with magnetic field when angular momentum is involved, and the change in frequency is related to the applied magnetic field as

$$\Delta E = h\Delta f = g_J \mu_B M_J B. \tag{A.1}$$

Here, $M_J = \pm 1$ or 0 is the magnetic quantum number of the excited state, and the Landé g-factor $g_J = 3/2$. As the magnetic field strength is increased, the degeneracy of the $^3P_1$ state is lifted and atoms absorb different frequencies of the 689 nm laser corresponding to their energy. This phenomenon is known as the Zeeman shift. Figure A.1 shows the results of this effect.

From this study, the y-axis trim coils used for the experiment found in this thesis are calibrated to cause a 0.6 MHz frequency shift with 0.9 A; this gives a field of 0.32 G per 1 A of current.

A.2 Time-of-flight Effect

Lineshapes also shift because of the Doppler effect. This effect is seen when atoms falling in the presence of gravity interact with the six beams from the 689 nm laser. That means that the atoms see three sets of beams with different frequencies because

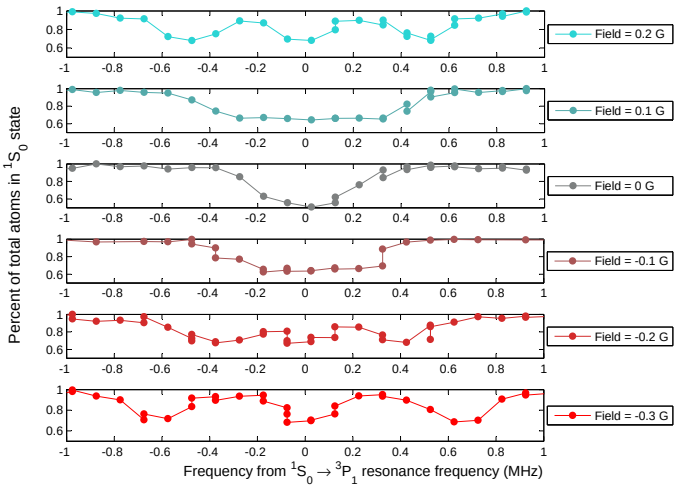

Figure A.1 Effect of external magnetic field on the linewidth of the $^1S_0 \rightarrow {}^3P_1$ transition. The frequency shift increases proportionally to the magnetic field. This behavior is expected due to Zeeman splitting.

of the Doppler shift due to their motion. Therefore, different velocity groups of atoms absorb the set of laser beams whose frequency appears on resonance with the atom's transition frequency. The frequency shift is related to the atom's velocity through

$$\Delta f = \frac{\overrightarrow{k} \cdot \overrightarrow{v}}{2\pi}. \tag{A.2}$$

$\overrightarrow{k}$ corresponds to the laser beam wave vector.

In order to study the fall of the atoms, the delay time τ_d between MOT cooling and the interaction of the 689 nm laser with the Sr atoms was varied. The delay times ranged from 1 ms to 30 ms. The different delay times give the atoms different amounts of time to accelerate due to gravity. This Doppler effect is seen in Figure A.2.

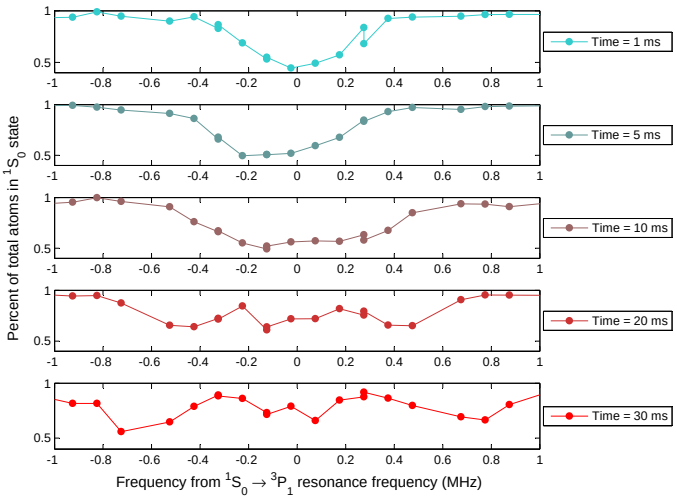

Figure A.2 Doppler effect on the linewidth of the $^1S_0 \rightarrow {}^3P_1$ transition due to atoms falling because of gravitational acceleration. The six MOT beams comprise the interaction beams, and so the falling atoms see sets of beams with three different frequencies.

A.3 Power Effect

Finding what is the narrowest possible line for this transition is probably the most informative effect studied. To perform this type of study, the $m_J = 0$ Zeeman sublevel was subjected to different 689 nm laser power levels during the interaction time τ_s. The temperature of the red MOT cloud for these experiments was about 5-10 μK.

The dominant contributions to the linewidth broadening of the $^1S_0 \rightarrow {}^3P_1$ transition for this experiment are Doppler broadening and laser power broadening. At a temperature of 10 μK, the spectrum of an atom's laser absorption has a $1/e$ Doppler full width of about 130 kHz. The total peak intensity on the atoms ranges from about 200 μW/cm^2 to 2.7 mW/cm^2. Since the saturation of the $^1S_0 \rightarrow {}^3P_1$ transition is 3 μW/cm^2, power broadening is present for these intensities. The results for the power

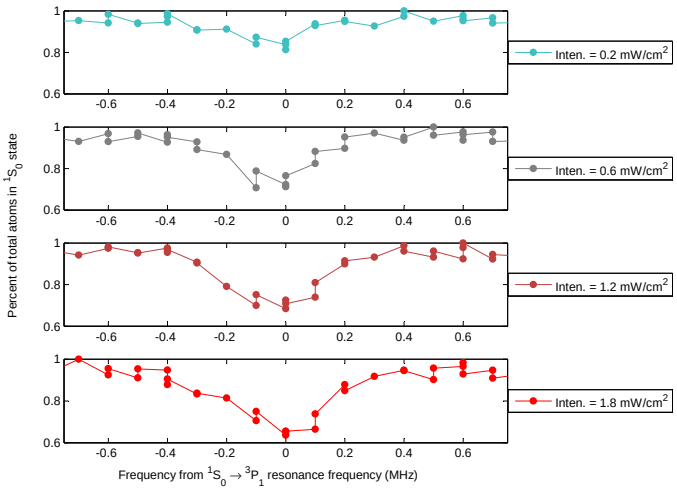

Figure A.3 Effect of laser power on linewidth of $^1S_0 \rightarrow {}^3P_1$ transition. The saturation intensity for the $^1S_0 \rightarrow {}^3P_1$ is 3 μW/cm^{-2}. Doppler broadening of the natural linewidth is the dominant contributor to the spectrum linewidth, and is comparable to the 689 nm laser linewidth.

study are shown in Figure A.3.

Analyzing these linewidth profiles allows one to set an upper limit on the 689 nm laser linewidth. Doppler broadening on the order of 130 kHz dominates the broadening for the lower laser intensities. With this, one sees that the Doppler broadening of the transition linewidth and the laser linewidth are comparable. It is straightforward to extract a quantitative value for the laser linewidth using a Voight profile, but this was not done for this thesis.

References

1. H. Dehmelt. *Bull. Am. Phys. Soc.*, 20:60, 1975.

2. H. Dehmelt. In F. T. Arecchi, F. Strumia, and H. Walther, editors, *Advances in Laser Spectroscopy*, volume 95 of *NATO Advanced Study Institute Series*, pages 153–187. Plenum Press, New York, 1983.

3. H. J. Metcalf and P. van der Straten. *Laser Cooling and Trapping*. Springer-Verlag New York, 1999.

4. T. Kurosu and F. Shimizu. Laser cooling and trapping of calcium and strontium. *Jpn J. Appl. Phys.*, 29(11):L2127, 1990.

5. H. Katori, T. Ido, Y. Isoya, and M. Kuwata-Gonokami. Magneto-optical trapping and cooling of strontium atoms down to the photon recoil temperature. *Phys. Rev. Lett.*, 82(6):1116, 1999.

6. J. L. Hall, M. Zhu, and P. Buch. Prospects for using laser-prepared atomic fountains for optical frequency standards applications. *J. Opt. Soc. Am. B*, 6(11):2194, 1989.

7. M. Machholm, P. S. Julienne, and K. Suominen. Calculations of collisions between cold alkaline-earth-metal atoms in a weak laser field. *Phys. Rev. A*, 64:033425, 2001.

8. S. B. Nagel, P. G. Mickelson, A. D. Saenz, Y. N. Martinez, Y. C. Chen, T. C. Killian, P. Pellegrini, and R. Côté. Photoassociative spectroscopy at long range in ultracold strontium. *Phys. Rev. Lett.*, 94:083004, 2005.

9. W. H. Parkinson, E. M. Reeves, and F. S. Tomkins. Neutral calcium, strontium and barium: determination of f values of the principal series by the hook method. *J. Phys. B: Atom. Molec. Phys.*, 9(2):157, 1976.

10. F. Ackermann, M. Baumann, and J. Gayler. Messung der lebensdauer des zustandes 5s 5p $^3P_1$ von strontium. *Z. Naturforsch., Teil A*, 21:664, 1966.

11. R. Drozdowski, M. Ignaciuk, J. Kwela, and J. Heldt. Radiative lifetimes of the lowest $^3P_1$ metastable states of Ca and Sr. *Z. Phys. D*, 41:125, 1997.

12. S. G. Porsev, M. G. Kozlov, and Yu. G. Rakhlina. High-precision calculations of the $^{3,1}P_1^0 \rightarrow {}^1S_0$ $E1$ amplitudes for magnesium, calcium, and strontium. *JETP Letters*, 72(12):595, 2000.

13. S. G. Porsev, M. G. Kozlov, Yu. G. Rakhlina, and A. Derevianko. Many-body calculations of electric-dipole amplitudes for transitions between low-lying levels of Mg, Ca, and Sr. *Phys. Rev. A*, 64:012508, 2001.

14. I. M. Savukov and W. R. Johnson. Combined configuration-interaction and many-body-perturbation-theory calculations of energy levels and transition amplitudes in Be, Mg, Ca, and Sr. *Phys. Rev. A*, 65:042503, 2002.

15. R. Santra, K. V. Christ, and C. H. Greene. Properties of metastable alkaline-earth-metal atoms calculated using an accurate effective core potential. *Phys. Rev. A*, 69:042510, 2004.

16. C. E. Moore. *Atomic Energy Levels*, volume II. United States Dept. of Commerce, National Bureau of Standards, Washington, D.C., 1952.

17. Yu. Ralchenko, A. E. Kramida, and J. Reader. NIST Atomic Spectra Database. http://physics.nist.gov/PhysRefData/ASD/index.html, visited April 5, 2005.

18. R. Marrus and P. J. Mohr. In D. R. Bates and B. Bederson, editors, *Advances in Atomic and Molecular Physics*, volume 14, pages 181–224. Academic Press, New York, 1978.

19. Y. Castin, H. Wallis, and J. Dalibard. Limit of doppler cooling. *J. Opt. Soc. Am. B*, 6(11):2046–2057, 1989.

20. T. H. Loftus, T. Ido, A. D. Ludlow, M. M. Boyd, and J. Ye. Narrow line cooling: Finite photon recoil dynamics. *Phys. Rev. Lett.*, 93:073003, 2004.

21. K. R. Vogel, T. P. Dinneen, A. Gallagher, and J. L. Hall. Narrow-line doppler cooling of strontium to the recoil limit. *IEEE Trans. Instrum. Meas.*, 48:618, 1999.

22. T. Binnewies, G. Wilpers, U. Sterr, F. Riehle, J. Helmcke, T. E. Mehlstaubler, E. M. Rasel, and W. Ertmer. Doppler cooling and trapping on forbidden transitions. *Phys. Rev. Lett.*, 87:123002, 2001.

23. C. W. Oates, F. Bondu, R. W. Fox, and L. Hollberg. A diode-laser optical frequency standard based on laser-cooled Ca atoms: Sub-kilohertz spectroscopy by optical shelving detection. *Eur. Phys. J. D*, 7:449, 1999.

24. Th. Udem, S. A. Diddams, K. R. Vogel, C. W. Oates, E. A. Curtis, W. D. Lee, W. M. Itano, R. E. Drullinger, J. C. Bergquist, and L. Hollberg. Absolute frequency measurements of the Hg^+ and Ca optical clock transitions with a femtosecond laser. *Phys. Rev. Lett.*, 86:4996, 2001.

25. G. Wilpers, T. Binnewies, C. Degenhardt, U. Sterr, J. Helmcke, and F. Riehle. Optical clock with ultracold neutral atoms. *Phys. Rev. Lett.*, 89:230801, 2002.

26. M. Takamoto and H. Katori. Spectroscopy of the $^1S_0$ - $^3P_0$ clock transition of ^{87}Sr in an optical lattice. *Phys. Rev. Lett.*, 91:223001, 2003.

27. T. Ido and H. Katori. Recoil-free spectroscopy of neutral Sr atoms in the lamb-dicke regime. *Phys. Rev. Lett.*, 91:053001, 2003.

28. A. Clairon, C. Salomon, S. Guellati, and W. D. Phillips. Ramsey resonance in a zacharias fountain. *Europhys. Lett.*, 16:165, 1991.

29. P. G. Mickelson, Y. N. Martinez, A. D. Saenz, S. B. Nagel, Y. C. Chen, T. C. Killian, P. Pellegrini, and R. Cote. Photoassociative spectroscopy and the s-wave scattering lengths of ^{86}Sr and ^{88}Sr. Submitted, *Phys. Rev. Lett.*, 2005.

30. T. Ido, Y. Isoya, and H. Katori. Optical-dipole trapping of Sr atoms at a high phase-space density. *Phys. Rev. A*, 61:061403, 2000.

31. Y. Takasu, K. Maki, K. Komori, T. Takano, K. Honda, M. Kumakura, T. Yabuzaki, and Y. Takahashi. Spin-singlet bose-einstein condensation of two-electron atoms. *Phys. Rev. Lett.*, 91:040404, 2003.

32. J. Migdalek and W. E. Baylis. Core-polarization-corrected multiconfiguration dirac-fock oscillator strengths and excitation energies for the 5s^2 $^1S_0$ - 5s5p $^3P_1$, $^1P_1$ transitions in Sr I and Y II spectra. *Can. J. Phys.*, 65:1612, 1987.

33. J. Bruneau. Correlation and relaxation effects in ns^2-nsnp transitions. *J. Phys. B: At. Mol. Phys.*, 17:3009, 1984.

34. S. R. Langhoff, C. W. Bauschlicher Jr., and H. Partridge. On the validity of the landé interval rule in the alkaline earth atoms. *Int. J. Quantum. Chem.*, S18:457, 1984.

35. G. Ritter and U. Eichmann. Lifetime of the Ca$^+$ $3^2D_{5/2}$ level from quantum jump statistics of a single laser-cooled ion. *J. Phys. B: At. Mol. Opt. Phys.*, 30:L141, 1997.

36. W. Nagourney, J. Sandberg, and H. Dehmelt. Shelved optical electron amplifier: Observation of quantum jumps. *Phys. Rev. Lett.*, 56:2797, 1986.

37. D. J. Wineland, J. C. Bergquist, W. M. Itano, and R. E. Drullinger. Double-resonance and optical-pumping experiments on electromagnetically confined, laser-cooled ions. *Opt. Lett.*, 5:245–247, 1980.

38. R. J. Cook and H. J. Kimble. Possibility of direct observation of quantum jumps. *Phys. Rev. Lett.*, 54:1023, 1985.

39. M. Knoop, C. Champenois, G. Hagel, M. Houssin, C. Lisowski, M. Vedel, and F. Vedel. Metastable level lifetimes from electron-shelving measurements with ion clouds and single ions. *arXiv:physics/0309094*, 2004.

40. W. M. Itano, J. C. Bergquist, R. G. Hulet, and D. J. Wineland. Radiative decay rates in Hg^+ from observations of quantum jumps in a single ion. *Phys. Rev. Lett.*, 59:2732, 1987.

41. M. Yasuda and H. Katori. Lifetime measurement of the $^3P_2$ metastable state of strontium atoms. *Phys. Rev. Lett.*, 92:153004, 2004.

42. R. Blatt and P. Zoller. Quantum jumps in atomic systems. *Eur. J. Phys.*, 9:250, 1988.

43. S. B. Nagel, C. E. Simien, S. Laha, P. Gupta, V. S. Ashoka, and T. C. Killian. Magnetic trapping of metastable $^3P_2$ atomic strontium. *Phys. Rev. A*, 86:011401, 2003.

44. T. C. Killian, Y. C. Chen, P. Gupta, S. Laha, Y. N. Martinez, P. G. Mickelson, S. B. Nagel, A. D. Saenz, and C. E. Simien. Absorption imaging and spectroscopy of ultracold neutral plasmas. *J. Phys. B: At. Mol. Opt. Phys.*, 38:S351, 2004.

45. J. K. Crane, M. J. Shaw, and R. W. Presta. Measurement of the cross sections for collisional broadening of the intercombination transitions in calcium and strontium. *Phys. Rev. A*, 49(3):1666, 1994.

46. L. R. Hunter, W. A. Walker, and D. S. Weiss. Observation of an atomic stark-electric-quadrupole interference. *Phys. Rev. Lett.*, 56:823, 1986.

47. D. Husain and J. Schifino. Kinetic study of $Sr(5^3P_J)$ by time-resolved emission, $5^3P_1 \rightarrow 5^1S_0 + h\nu$ ($\lambda = 689.3$ nm), following dye-laser excitation. *J. Chem. Soc., Faraday Trans. 2*, 80:321, 1984.

48. E. N. Borisov, N. P. Penkin, and T. P. Redko. Diffusion coefficients of $5^3P_{0,1,2}$ strontium atoms in argon. *Opt. Spectrosc. (USSR)*, 59:426, 1985.

49. D. Husain and G. Roberts. A kinetic investigation of the collisional behaviour of $Sr(5^3P_J)$ with H_2 and D_2 over the temperature range 725-1100 K, studied by time-resolved atomic emission at $\lambda = 689.3$ nm [$Sr(5^3P_1) \rightarrow Sr(5^1S_0) + h\nu$] following pulsed dye-laser excitation. *J. Chem. Soc., Faraday Trans. 2*, 81:1085, 1985.

50. D. Husain and G. Roberts. Radiative lifetimes, diffusion and energy pooling of Sr(5s5p(^3P_J)) and Sr(5s4d($^1D_2$)) studied by time-resolved atomic emission following pulsed dye-laser excitation. *Chem. Phys.*, 127:203, 1988.

51. J. F. Kelly, M. Harris, and A. Gallagher. Collisional transfer within the Sr($5^3P_J^0$) multiplet due to nearly adiabatic collisions with noble gases. *Phys. Rev. A*, 37:2354, 1988.

52. J. Migdalek and M. Stanek. The spin-allowed and spin-forbidden $5s^2\ ^1S_0$-5s5p $^1P_1$, $^3P_1$ transitions in strontium isoelectronic sequence. *Z. Phys. D*, 27:9, 1993.

53. R. C. Hilborn. Einstein coefficients, cross sections, f values, dipole moments, and all that. *Am. J. Phys.*, 50:982, 1982.